

# Improving the $J/\psi$ Production Baseline at RHIC and the LHC

R. Vogt and R.E. Nelson

Lawrence Livermore National Laboratory, Livermore, CA 94551, USA  
Physics Department, University of California, Davis, CA 95616, USA

- $pp$  Collisions
- $pA$  and  $dA$  Collisions

# Color Evaporation Model

All quarkonium states are treated like  $Q\bar{Q}$  ( $Q = c, b$ ) below  $H\bar{H}$  ( $H = D, B$ ) threshold; mass and scale parameters fixed from open  $Q\bar{Q}$  calculation

Distributions for all quarkonium family members similar, modulo decay feed down, production ratios should be independent of  $\sqrt{s}$

Gavai *et al.* calculated complete  $J/\psi$   $p_T$  distribution starting from exclusive NLO  $Q\bar{Q}$  production code by Mangano *et al.*

At LO,  $gg \rightarrow Q\bar{Q}$  and  $q\bar{q} \rightarrow Q\bar{Q}$ ; NLO add  $gq \rightarrow Q\bar{Q}q$

$$\sigma_Q^{\text{CEM}} = F_Q \sum_{i,j} \int_{4m_Q^2}^{4m_H^2} d\hat{s} \int dx_1 dx_2 f_{i/p}(x_1, \mu^2) f_{j/p}(x_2, \mu^2) \hat{\sigma}_{ij}(\hat{s}) \delta(\hat{s} - x_1 x_2 s)$$

Main uncertainties arise from choice of PDFs, heavy quark mass, renormalization ( $\alpha_s$ ) and factorization (evolution of PDFs) scales

Inclusive  $F_Q$  fixed by comparison of NLO calculation of  $\sigma_Q^{\text{CEM}}$  to  $\sqrt{s}$  dependence of  $J/\psi$  and  $\Upsilon$  cross sections,  $\sigma(x_F > 0)$  and  $Bd\sigma/dy|_{y=0}$  for  $J/\psi$ ,  $Bd\sigma/dy|_{y=0}$  for  $\Upsilon$

Data and branching ratios used to separate the  $F_Q$ 's for each quarkonium state

Resonance	$J/\psi$	$\psi'$	$\chi_{c1}$	$\chi_{c2}$	$\Upsilon$	$\Upsilon'$	$\Upsilon''$	$\chi_b(1P)$	$\chi_b(2P)$
$\sigma_i^{\text{dir}}/\sigma_H$	0.62	0.14	0.6	0.99	0.52	0.33	0.20	1.08	0.84
$f_i$	0.62	0.08	0.16	0.14	0.52	0.10	0.02	0.26	0.10

Table 1: The ratios of the direct quarkonium production cross sections,  $\sigma_i^{\text{dir}}$ , to the inclusive  $J/\psi$  and  $\Upsilon$  cross sections, denoted  $\sigma_H$ , and the feed down contributions of all states to the  $J/\psi$  and  $\Upsilon$  cross sections,  $f_i$ , Digal *et al.*

# Determining the Uncertainty on the CEM Result

Previously took 'by eye' fit to  $Q\bar{Q}$  total cross section

Dates back to original Hard Probes Collaboration report in 1995 – only PDFs changed over time

Results shown here based on fitting mass and scale parameters at NLO to total charm cross section data and using same parameters to calculate  $J/\psi$  in CEM (with A.D. Frawley, FSU)

Define upper and lower bounds of theoretical values; the maximum and minimum may not come from the same set of parameters at a given energy or  $p_T$

The uncertainty band comes from the upper and lower limits of mass and scale uncertainties added in quadrature:

$$\sigma_{\max} = \sigma_{\text{cent}} + \sqrt{(\sigma_{\mu,\max} - \sigma_{\text{cent}})^2 + (\sigma_{m,\max} - \sigma_{\text{cent}})^2}$$

$$\sigma_{\min} = \sigma_{\text{cent}} - \sqrt{(\sigma_{\mu,\min} - \sigma_{\text{cent}})^2 + (\sigma_{m,\min} - \sigma_{\text{cent}})^2}$$

One final remark: there is no calculation of the polarization, would need to start from NLO polarized  $Q\bar{Q}$  production calculation

BTW, no prediction does not necessarily mean a flat distribution, it means there is no calculation

# Main Sources of Uncertainty

$\alpha_s$  changing rapidly, especially for  $\mu_R = \mu_0/2$

Results depend on choice of  $\mu_0$  in parton densities (lower  $\mu_0$  means smaller  $\alpha_s$  at low scales)

Low factorization scales result in unreliable results for gluon densities

Backwards evolution required for low scale ( $\mu_F = m, m/2$ ) charm production

At RHIC energies and higher, the gluon distribution with  $\mu_F = m/2$  turns over while the distribution with  $\mu_F = m$  is almost independent of  $x$  for  $x < 0.01$

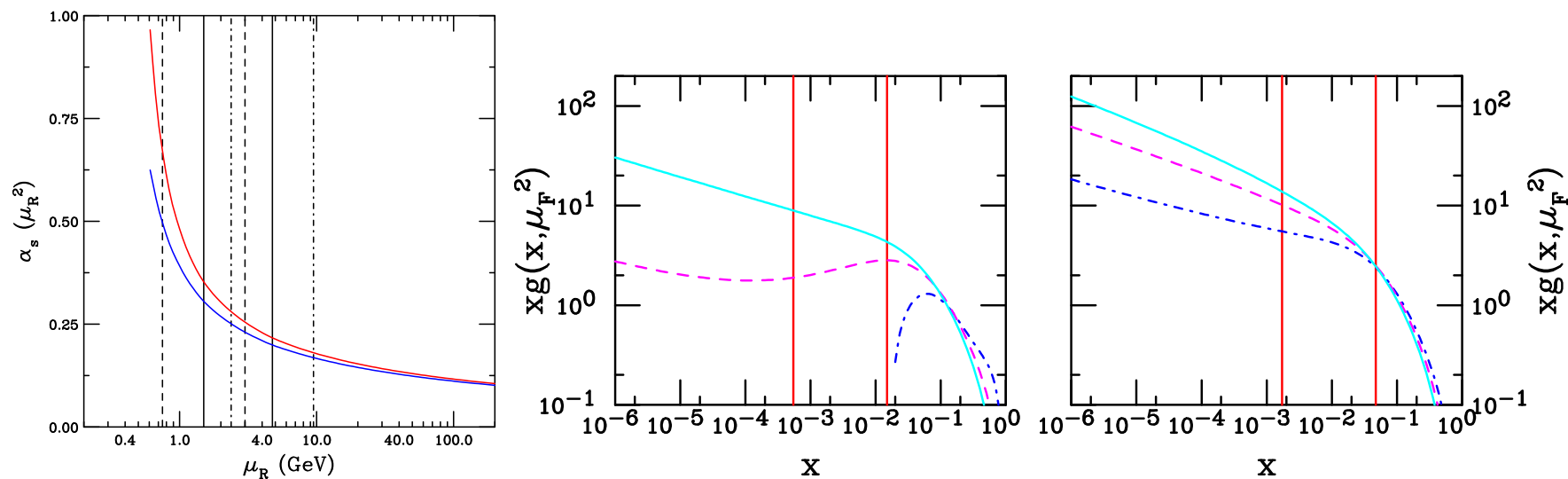


Figure 1: (Left) The running coupling constant for CTEQ6M (red) with  $\Lambda^{n_f=5} = 0.226$  GeV and for GRV98 (blue) with  $\Lambda^{n_f=5} = 0.1677$  GeV. The vertical bars are at  $\mu_R = 1.5$  and  $4.75$  GeV. (Right) The CTEQ6M parton densities as a function of  $x$  for  $\mu_F/m = 0.5$  (dot-dashed),  $\mu_F/m = 1$  (dashed) and  $\mu_F/m = 2$  (solid) for  $m = 1.5$  GeV (left-hand side) and  $4.75$  GeV (right-hand side). The vertical lines are at  $x = 2m/\sqrt{S}$  in  $\sqrt{S} = 200$  GeV and  $5.5$  TeV  $pp$  collisions at RHIC and the LHC.

# Large Uncertainties with FONLL Fiducial Parameters

With a given PDF set define a fiducial region of mass and scale that should encompass the true value – central mass and scale  $(m, \mu_F/m, \mu_R/m) = (1.5 \text{ GeV}, 1, 1)$ :

- For  $\mu_F = \mu_R = m$ , vary mass,  $1.3 < m < 1.7$ ;
- For  $m = 1.5 \text{ GeV}$ , vary scales independently within a factor of two:  
 $(\mu_F/m, \mu_R/m) = (1, 1), (2, 2), (0.5, 0.5), (0.5, 1), (1, 0.5), (1, 2), (2, 1)$ .

Low scales set limits on uncertainty ( $\mu_R/m = 0.5$  upper limit,  $\mu_F/m = 0.5$  lower limit)  
 Large combination of mass and scale uncertainty makes lower limit ill defined

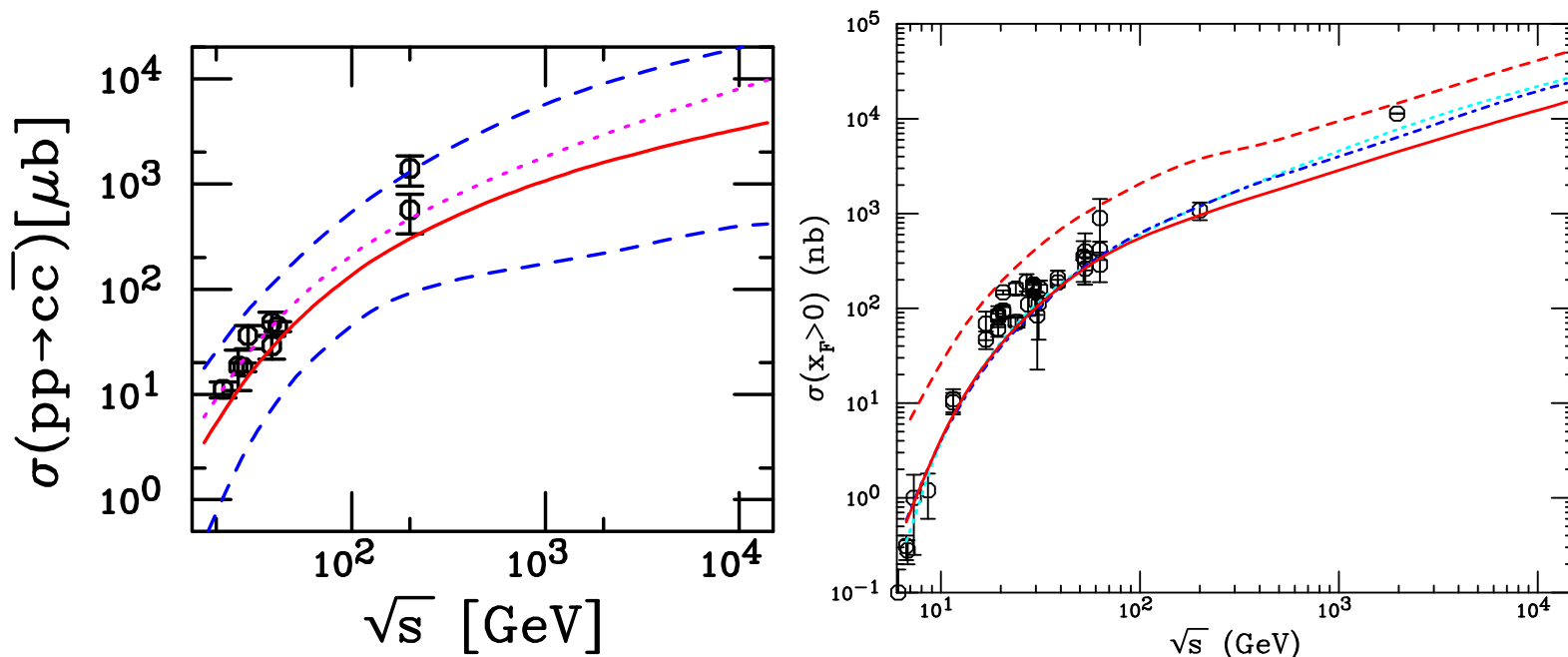


Figure 2: (Left) Uncertainty band formed from adding mass and scale uncertainties in quadrature. (Right) The solid and dashed red curves are the central value and upper limit for the  $J/\psi$  cross section. The solid cyan curve employs the MRST HO distributions while the dot-dashed blue curve is a result with CTEQ6M, both employing  $m_c = 1.2 \text{ GeV}$ .  $(\mu_F/m_T, \mu_R/m_T) = (2, 2)$ .

# Choosing $J/\psi$ Parameters by Fitting $\sigma_{c\bar{c}}$

$J/\psi$  parameters based on fits to NLO total  $c\bar{c}$  cross section – caveat: full NNLO cross section unknown, could still be large correction

Employ  $m = 1.27$  GeV, value of charm quark mass from lattice calculations at  $m(3\text{ GeV})$

Use subset of  $c\bar{c}$  total cross section data to fix best fit values of  $\mu_F/m$  and  $\mu_R/m$

Result with  $\Delta\chi^2 = 1$  gives uncertainty on scale parameters;  $\Delta\chi^2 = 2.3$  gives one standard deviation on total cross section

Range of  $\mu_R$  for given  $m$  is very narrow; range of  $\mu_F$  is rather broad, especially when RHIC cross sections are included

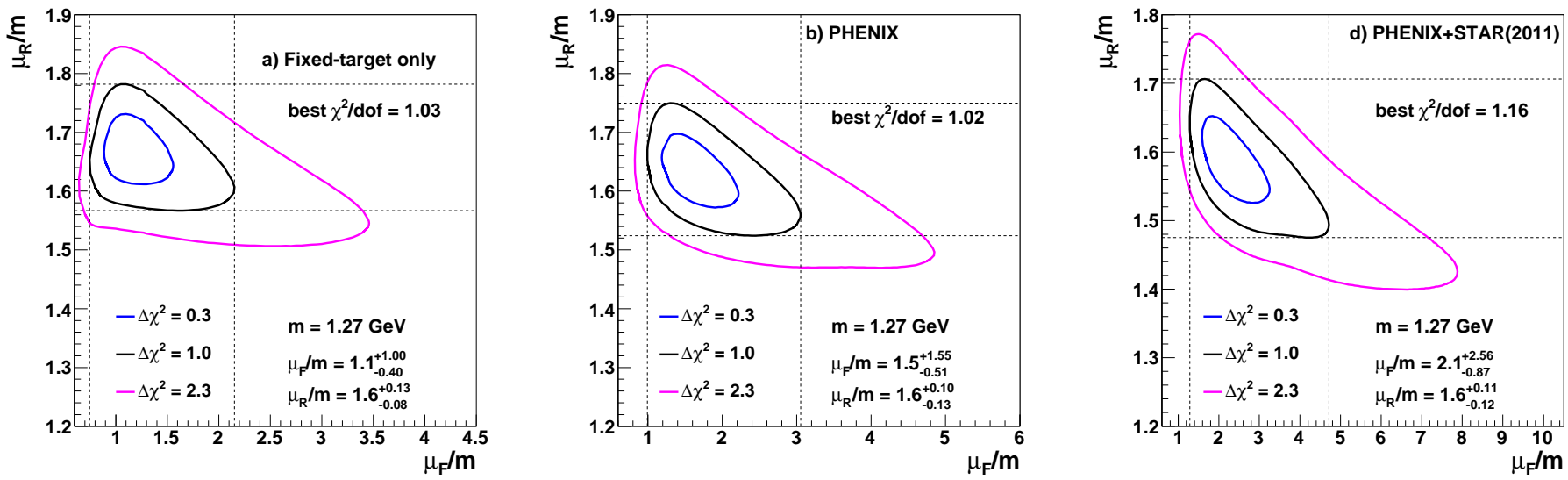


Figure 3: The  $\chi^2/\text{dof}$  contours for (left) fixed target data only, (center) including the PHENIX 200 GeV cross section, and (right) including the STAR 2011 cross section but excluding the STAR 2004 cross section. The best fit values are given for the furthest extent of the  $\Delta\chi^2 = 1$  contours.

# Energy Dependence of Fit Results

Fixed-target only fit (left) gives worst agreement with RHIC data and largest spread in total cross section (due to low factorization scales in fit region)

Including most recent STAR analysis with PHENIX data at  $\sqrt{s} = 200$  GeV gives strongest energy dependence and narrowest uncertainty region (right) than with PHENIX alone (center)

Remainder of results shown with fit to fixed-target + PHENIX + STAR (2011) on right-hand side

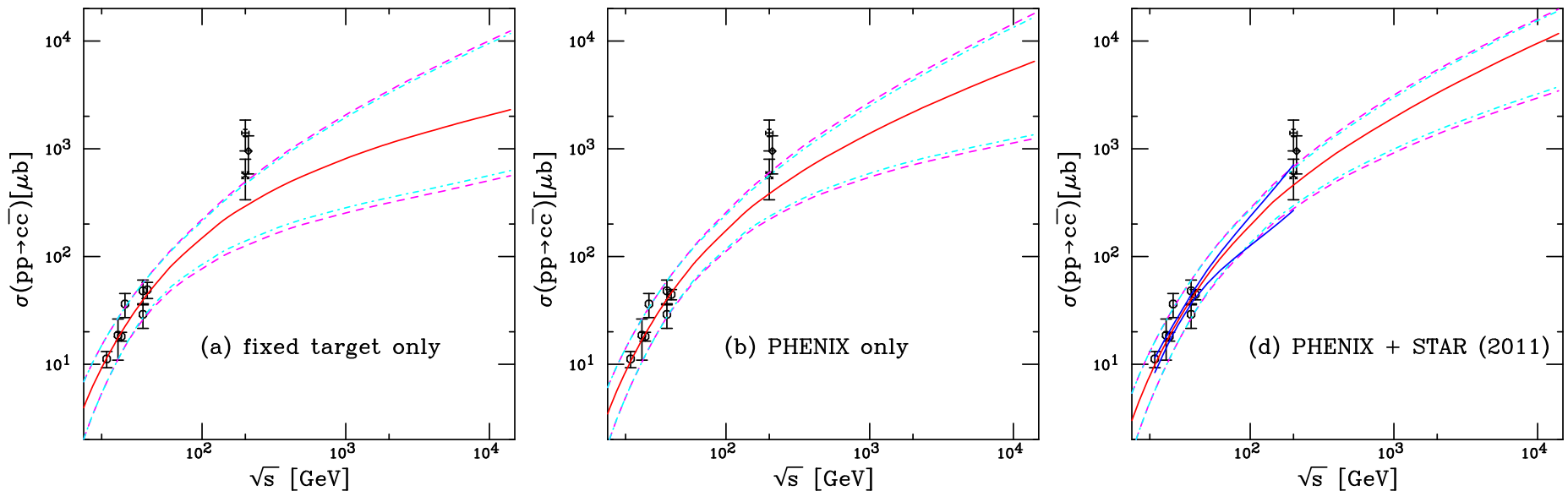


Figure 4: The energy dependence of the charm total cross section compared to data for (left) fixed target data only, (center) including the PHENIX 200 GeV cross section, and (right) including the STAR 2011 cross section but excluding the STAR 2004 cross section. The best fit values are given for the furthest extent of the  $\Delta\chi^2 = 1$  contours. The central value of the fit in each case is given by the solid red curve while the dashed magenta curves and dot-dashed cyan curves show the extent of the corresponding uncertainty bands. The dashed curves outline the most extreme limits of the band. On the bottom right, the solid blue curves in the range  $19.4 \leq \sqrt{s} \leq 200$  GeV represent the uncertainty obtained from the extent of the  $\Delta\chi^2 = 2.4$  contour of fit including STAR 2011 data.

# Results on ALICE Heavy Flavor Distributions

Excellent agreement with  $\sqrt{s} = 7$  TeV ALICE  $pp$  data

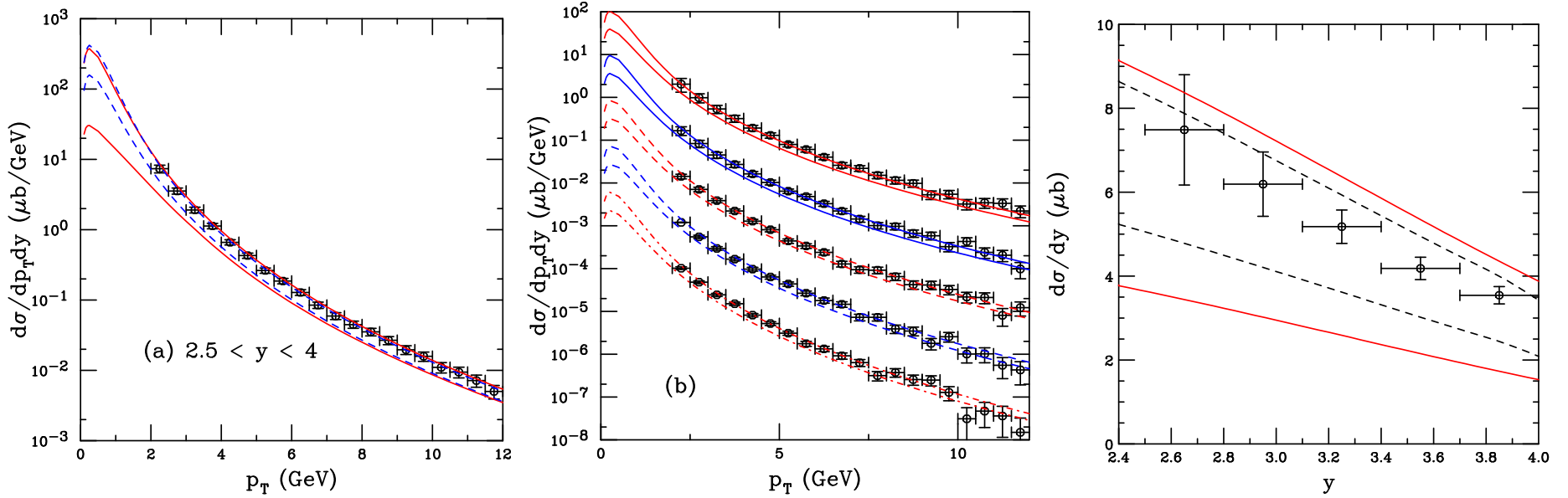


Figure 5: (Left) Comparison of the single lepton  $p_T$  distributions in the rapidity interval  $2.5 < y < 4$  at  $\sqrt{s} = 7$  TeV calculated with the FONLL set for charm (solid red) and the fitted set with  $m = 1.27$  GeV (dashed black). (Center) The contributions to the  $p_T$  distributions in (a) divided into rapidity bins, from top to bottom:  $2.5 < y < 2.8$  (solid red);  $2.8 < y < 3.1$  (solid blue);  $3.1 < y < 3.4$  (dashed red);  $3.4 < y < 3.7$  (dashed blue); and  $3.7 < y < 4$  (dot-dashed red). The top curves are shown at their calculated value, the others are scaled down by successive factors of 10 to separate them. (Right) The sum of the contributions are compared with the FONLL set for charm (solid red) and  $m = 1.27$  GeV (dashed black).

# $J/\psi$ Cross Sections from $c\bar{c}$ Fits

Take results of  $c\bar{c}$  fits, calculate NLO  $J/\psi$  cross section in CEM, fit scale factor  $F_C$   
 Energy dependence almost identical for  $\mu_F = 2m_T$ ,  $\sqrt{s}$  dependence generally better  
 CTEQ6M and CT10 have nearly same value of  $F_C$  so previous results compatible  
 with previous results

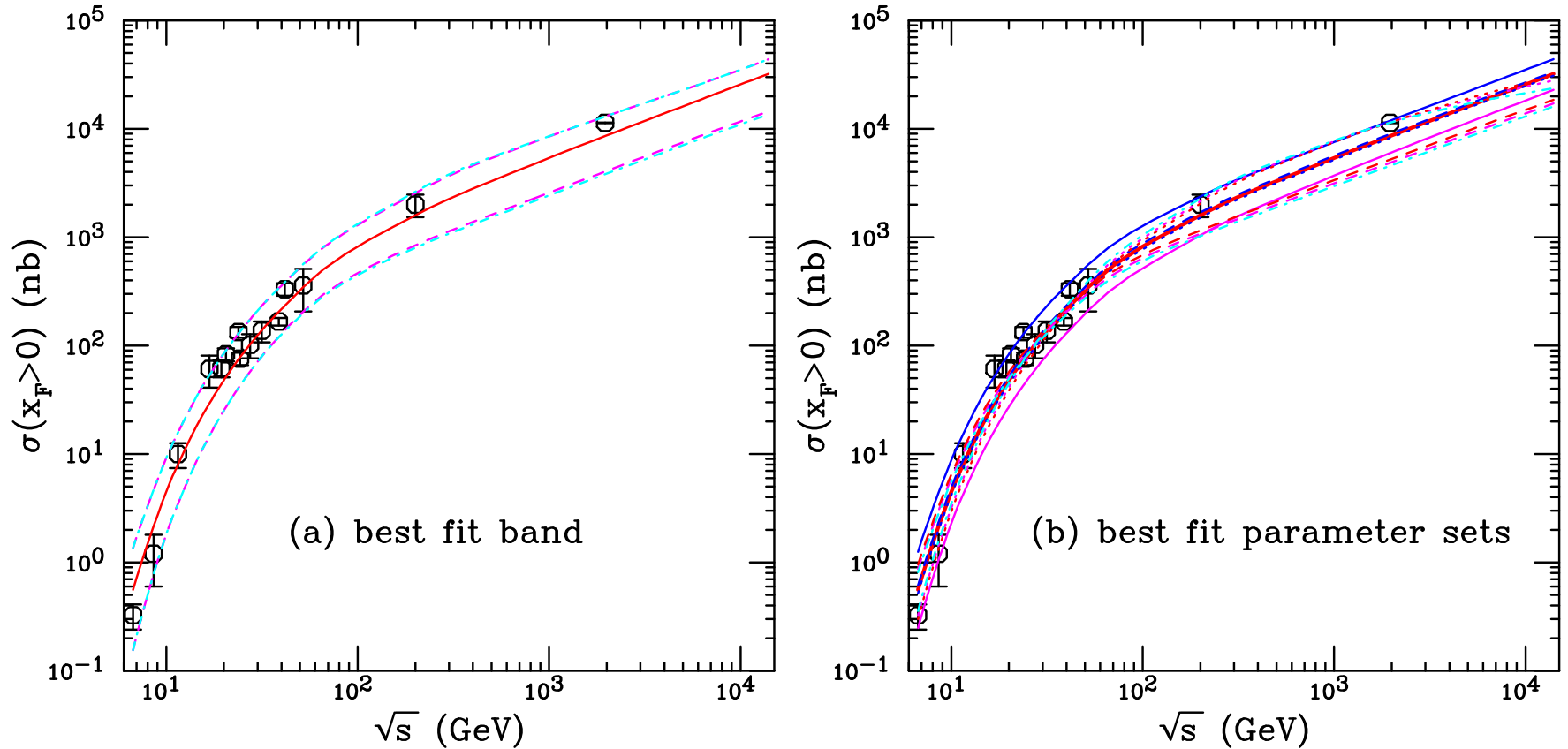


Figure 6: (Left) The uncertainty band on the forward  $J/\psi$  cross section. The dashed magenta curves and dot-dashed cyan curves show the extent of the corresponding uncertainty bands. The dashed curves outline the most extreme limits of the band. (Right) The components of the uncertainty band. The central value  $(m, \mu_F/m_T, \mu_R/m_T) = (1.27 \text{ GeV}, 2.10, 1.60)$  is given by the solid red curve. The solid blue and magenta curves outline the mass uncertainty with  $(1.18 \text{ GeV}, 2.10, 1.60)$  and  $(1.36 \text{ GeV}, 2.10, 1.60)$  respectively. The dashed curves outline the lower limits on the scale uncertainty:  $(\mu_F/m_T, \mu_R/m_T) = (2.10, 1.48)$  blue;  $(1.25, 1.60)$  magenta; and  $(1.25, 1.48)$  red. The dotted curves outline the upper limits on the scale uncertainty:  $(\mu_F/m_T, \mu_R/m_T) = (2.10, 1.71)$  blue;  $(1.25, 1.60)$  magenta; and  $(1.25, 1.48)$  red. The solid curves outline the central values:  $(\mu_F/m_T, \mu_R/m_T) = (2.10, 1.71)$  blue;  $(1.25, 1.60)$  magenta; and  $(1.25, 1.48)$  red.

# Comparison to RHIC $pp$ $J/\psi$ Data

CEM calculation reproduces shape of  $J/\psi$   $p_T$  and  $y$  distributions rather well considering that normalization is set from RHIC energies and below with only one parameter

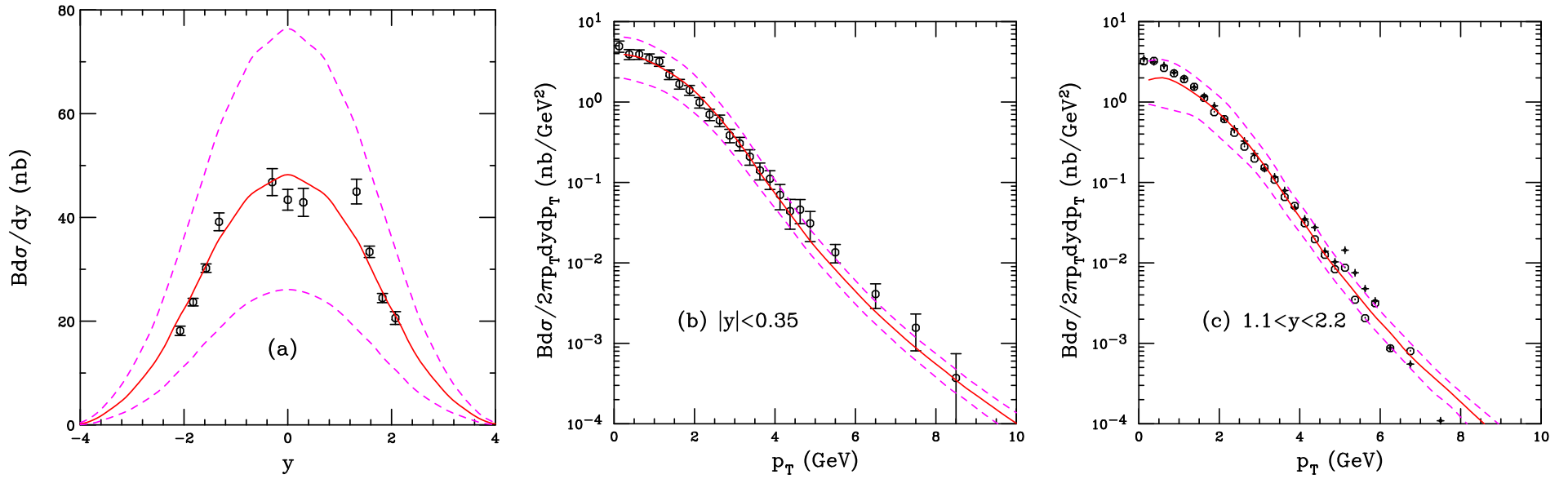


Figure 7: The  $J/\psi$  rapidity distribution (a) and the midrapidity (b) and forward rapidity (c)  $p_T$  distributions and their uncertainties. The results are compared to PHENIX  $pp$  measurements at  $\sqrt{s} = 200$  GeV. The solid red curve shows the central value while the dashed magenta curves outline the uncertainty band. A  $\langle k_T^2 \rangle$  kick of 1.19 GeV<sup>2</sup> is applied to the  $p_T$  distributions, as discussed in the text.

# Comparison to ALICE $pp$ Data

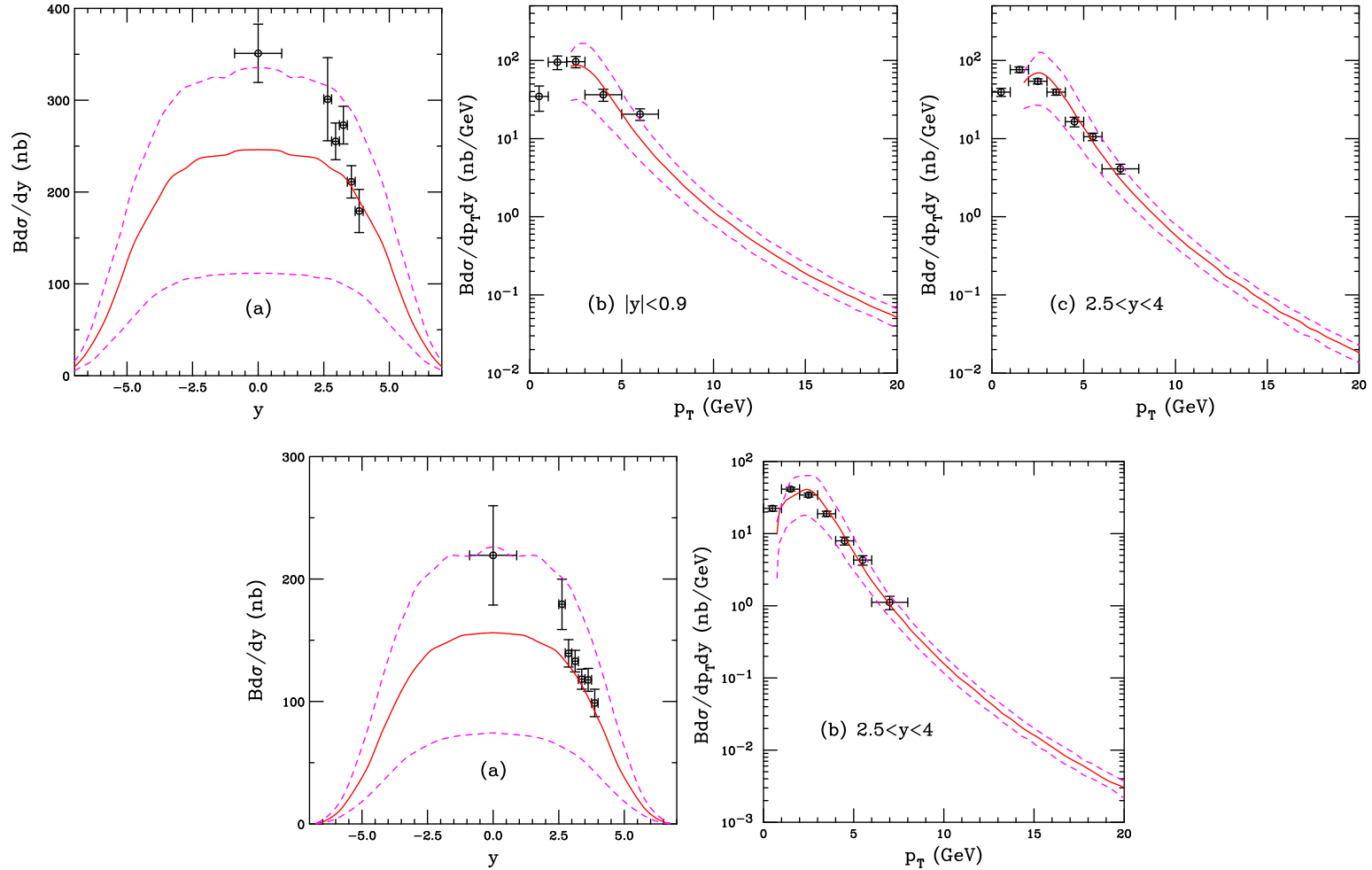


Figure 8: The  $J/\psi$  rapidity distribution (a) and the midrapidity,  $|y| < 0.9$  (b), and forward rapidity,  $2.5 < y < 4$  (c)  $p_T$  distributions at  $\sqrt{s} = 7$  TeV (top) and 2.76 TeV (bottom) and their uncertainties. The results are compared to the ALICE rapidity distribution as well as the  $p_T$  distributions. The solid red curve shows the central value while the dashed magenta curves outline the uncertainty band. A  $\langle k_T^2 \rangle$  kick of 1.49 GeV<sup>2</sup> is applied to the  $p_T$  distributions, as discussed in the text.

## *pA* and dA Production

# Medium Effects Important with Nuclear Target

Nuclear effects often parameterized as

$$\sigma_{pA} = \sigma_{pp} A^\alpha \quad \alpha(x_F, p_T)$$

For  $\sqrt{s_{NN}} \leq 40$  GeV and  $x_F > 0.25$ ,  $\alpha$  decreases strongly with  $x_F$  – only low  $x_F$  effects probed by SPS and RHIC rapidity coverage

Possible cold matter effects

- Nuclear Shadowing — initial-state effect on the parton distributions affecting total rate, important as a function of  $y/x_F$
- Energy Loss — initial-state effect, elastic scatterings of projectile parton before hard scattering creating quarkonium state, need to study Drell-Yan production to get a handle on the strength when shadowing included
- Intrinsic Charm — initial-state effect, if light-cone models correct, should only contribute to forward production, assumed to have different  $A$  dependence than normal  $J/\psi$  production
- Absorption — final-state effect, after  $c\bar{c}$  that forms the  $J/\psi$  has been produced, pair breaks up in matter due to interactions with nucleons

# Comparison of LO and NLO EPS09 Gluon nPDFs

Nuclear gluon density not as well constrained at finite scales as are quark distributions

LO EPS09 shadowing ratio has a wider antishadowing region and bigger uncertainty in EMC region ( $x > 0.3$ )

At low  $x$ ,  $x < 0.01$ , the uncertainty in shadowing is smaller at NLO

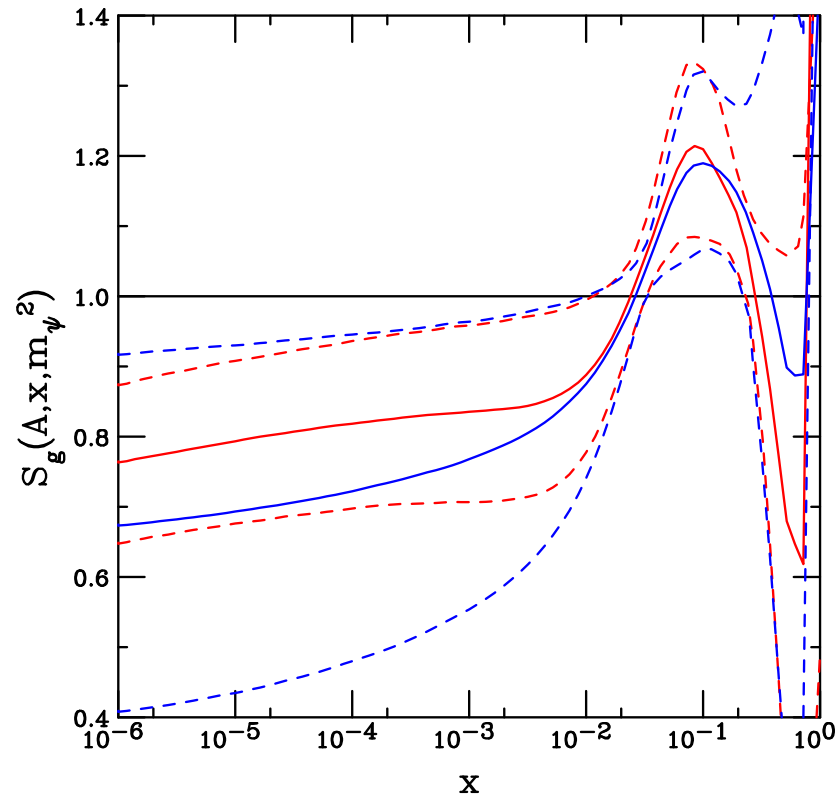


Figure 9: The modification of the gluon densities at LO (blue) and NLO (red) with EPS09, including uncertainties (dashed lines), calculated at  $m_\psi$ .

# Effects on the $J/\psi$ Cross Section at $\sqrt{s_{NN}} = 200$ GeV

Both ratios calculated in the CEM

Left side: calculated with LO EKS98 parameterization with both LO ( $2 \rightarrow 1$ ) and NLO ( $2 \rightarrow 2$ ) kinematics – ratios are the same within statistics

Right side: LO ratio (blue) calculated with EPS09 LO shadowing; NLO ratio is calculated with EPS09 NLO shadowing

Newer calculation shows a difference because the LO and NLO gluon shadowing is different with EPS09 and not well enough constrained to make the ratios more similar, as opposed to quark-dominated observables

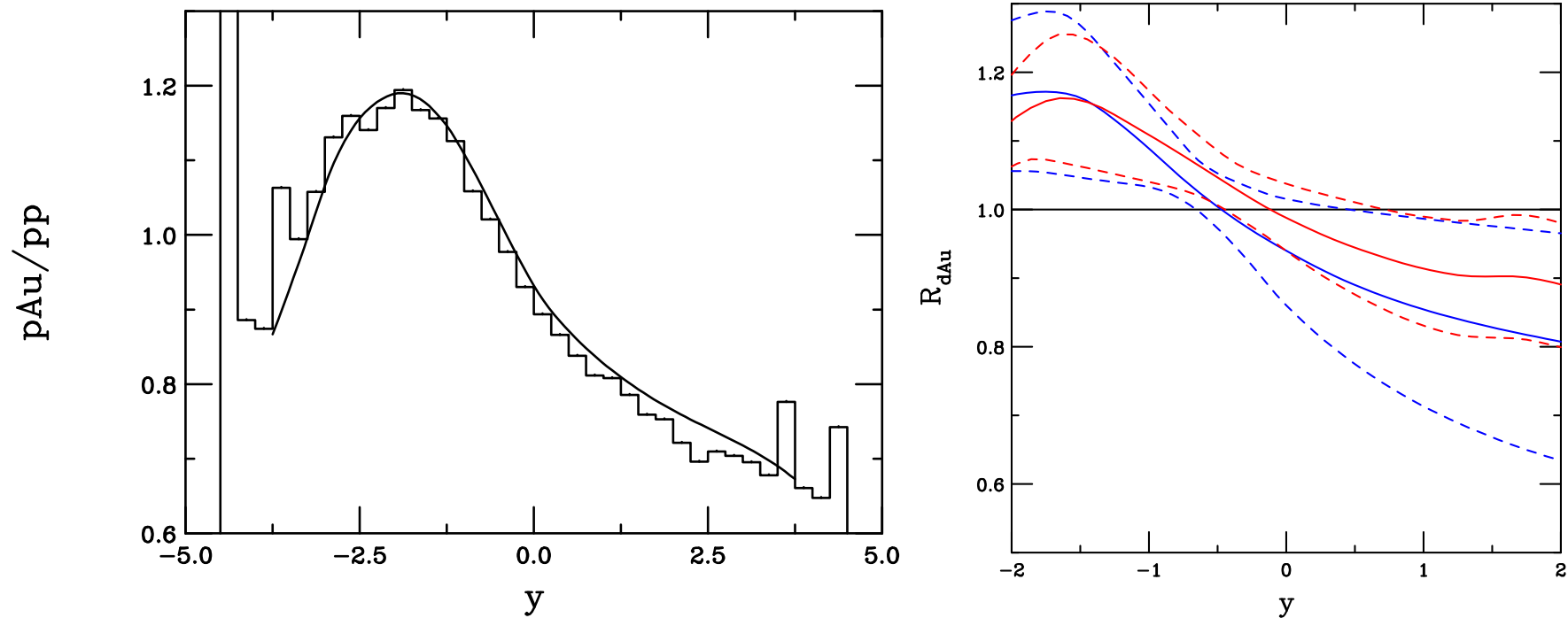


Figure 10: Left: The ratio  $R_{dAu}$  at  $\sqrt{s_{NN}} = 200$  GeV at LO and NLO with the EKS98 parameterization. Right: The LO and NLO calculations of  $R_{dAu}$ .

# NLO Scale Dependence Smaller than nPDF Dependence

Left side: Red band shows variation with EPS09 NLO shadowing; blue band takes central EPS09 set and presents mass and scale variations for that set

Center: variation in EPS09 LO shadowing due to varying charm quark mass  $1.18 < m < 1.36$  GeV

Right: variation in EPS09 LO shadowing with  $\mu_F/m = 1.25, 2.10$  and  $4.65$ , limits of factorization

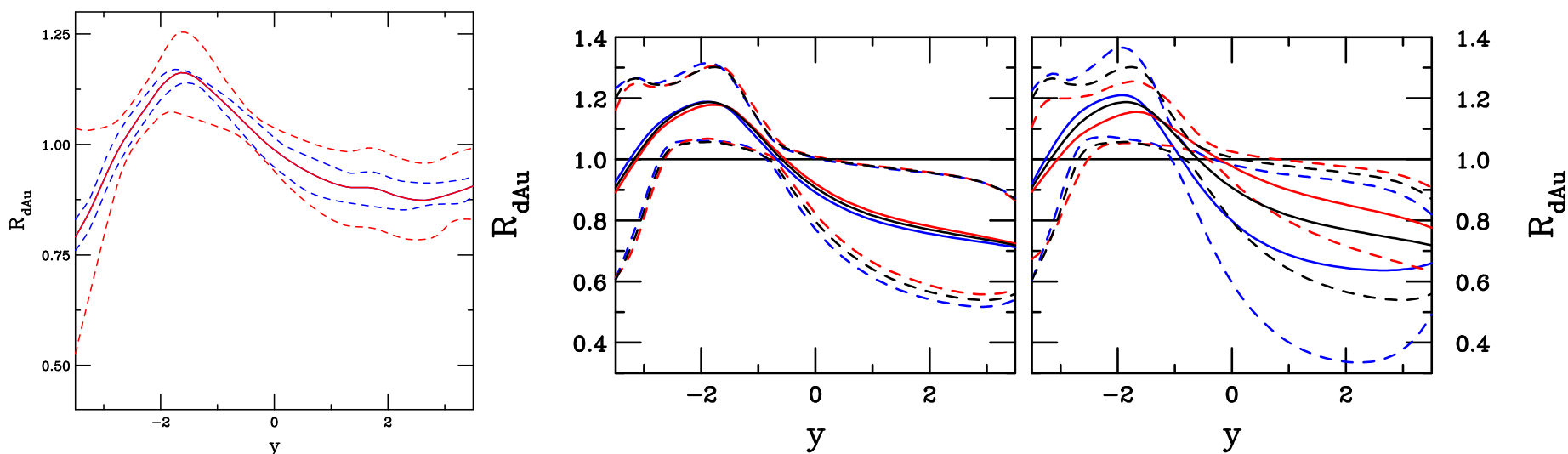


Figure 11: Left: The scale variation of  $R_{dAu}$  with the central EPS09 set (blue) compared to the EPS09 variation for the central parameter set (red). Right: The EPS09 uncertainty band in 200 GeV d+Au collisions at RHIC for (left)  $m = 1.18$  (blue), 1.27 (black), and 1.36 (red) GeV with the central scale values and for (right)  $m = 1.27$  GeV with  $\mu_F/m = 2.8$  (black), 1.41 (blue) and 5.91 (red).

# NLO vs LO Shadowing in $AA$ Collisions

Left side: Red band shows variation with EPS09 NLO shadowing; blue band takes central EPS09 set and presents mass and scale variations for that set

Center: variation in EPS09 LO shadowing due to varying charm quark mass  $1.18 < m < 1.36$  GeV

Right: variation in EPS09 LO shadowing with  $\mu_F/m = 1.25, 2.10$  and  $4.65$ , limits of factorization

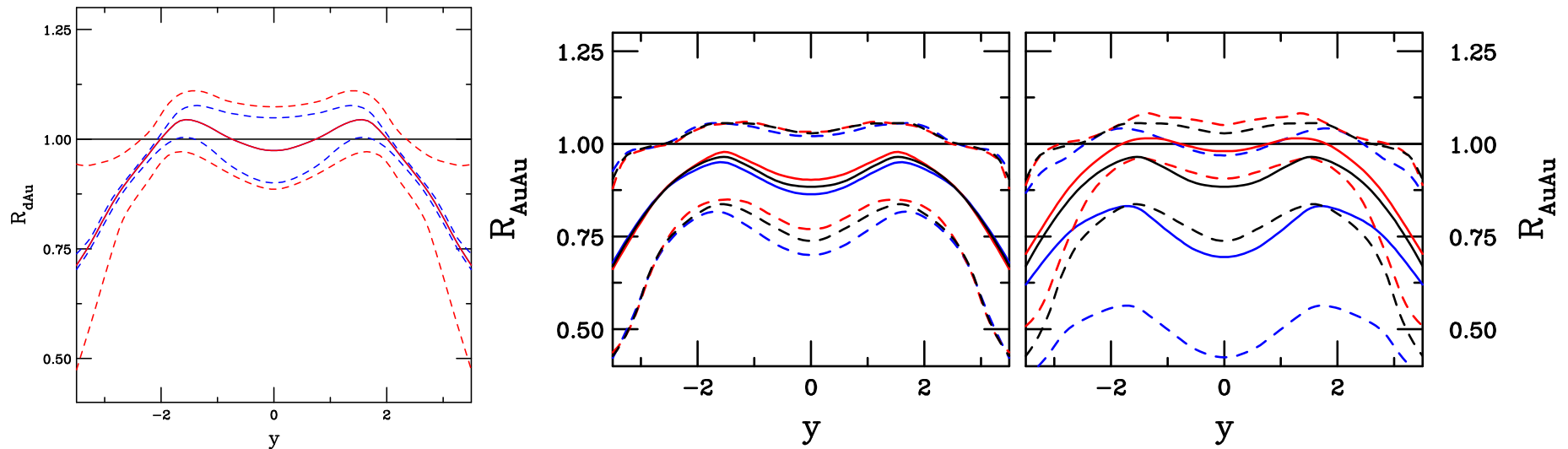


Figure 12: Left: The scale variation of  $R_{AuAu}$  with the central EPS09 set (blue) compared to the EPS09 variation for the central parameter set (red). Right: The EPS09 uncertainty band in 200 GeV Au+Au collisions at RHIC for (left)  $m = 1.18$  (blue), 1.27 (black), and 1.36 (red) GeV with the central scale values and for (right)  $m = 1.27$  GeV with  $\mu_F/m = 2.8$  (black), 1.41 (blue) and 5.91 (red).

# Extrinsic vs. Intrinsic $J/\psi$ Production

Both ratios calculated in the CEM

LO CEM calculation on left equivalent to 'intrinsic' calculation with  $p_T = 0$  on right-hand side

Including average  $p_T$  in scale of LO CEM shifts shape somewhat, amount of shift depends on assumed scale

'Extrinsic' calculation is LO CSM, results similar to central value of NLO CEM result on left-hand side

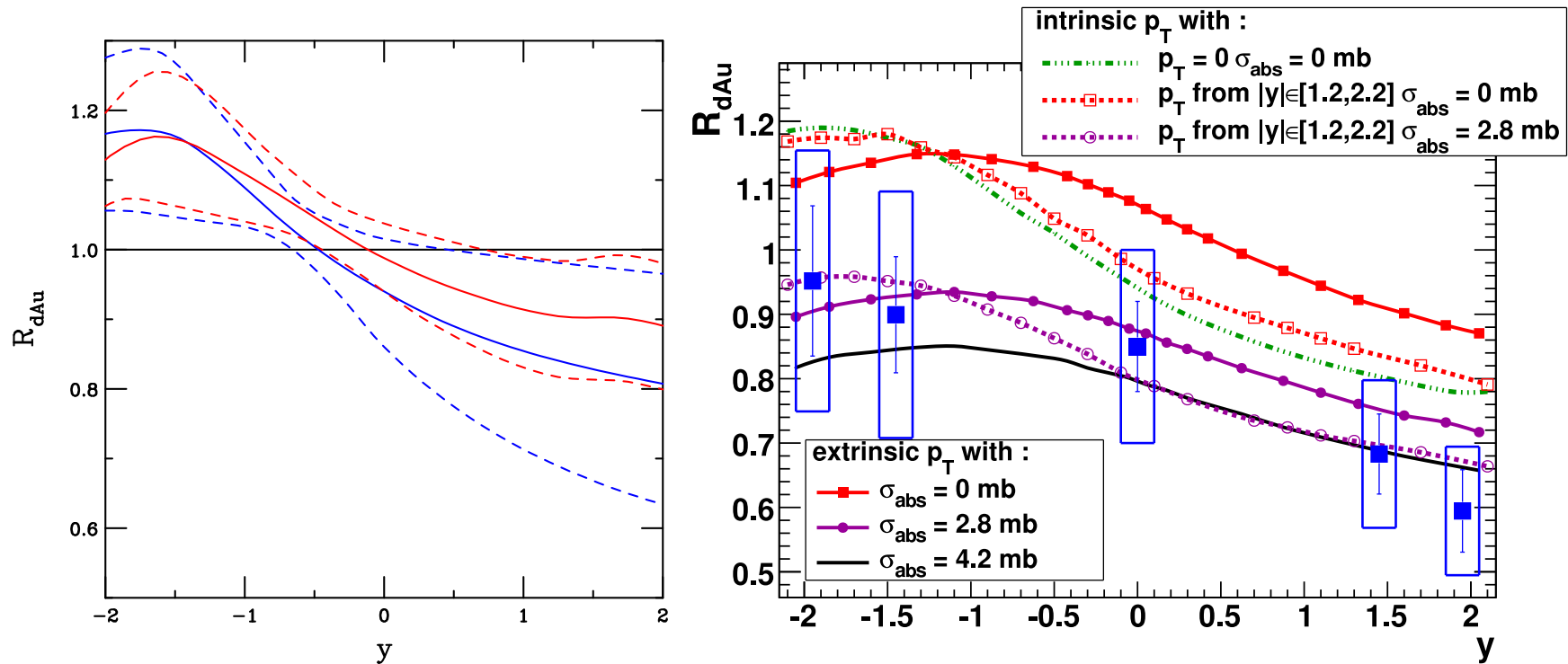


Figure 13: Left: The  $\pi^0$  cross section in d+Au collisions at  $\sqrt{s_{NN}} = 200$  GeV at LO and NLO. Right: The LO and NLO calculations of  $R_{dAu}$ .

# $p_T$ Dependence of Shadowing Accessible at NLO

The  $pp$ ,  $d+Au$  and  $Au+Au$   $p_T$  distributions calculated with same intrinsic  $k_T$  kick  
Scale dependence again reduced relative to nPDF uncertainties

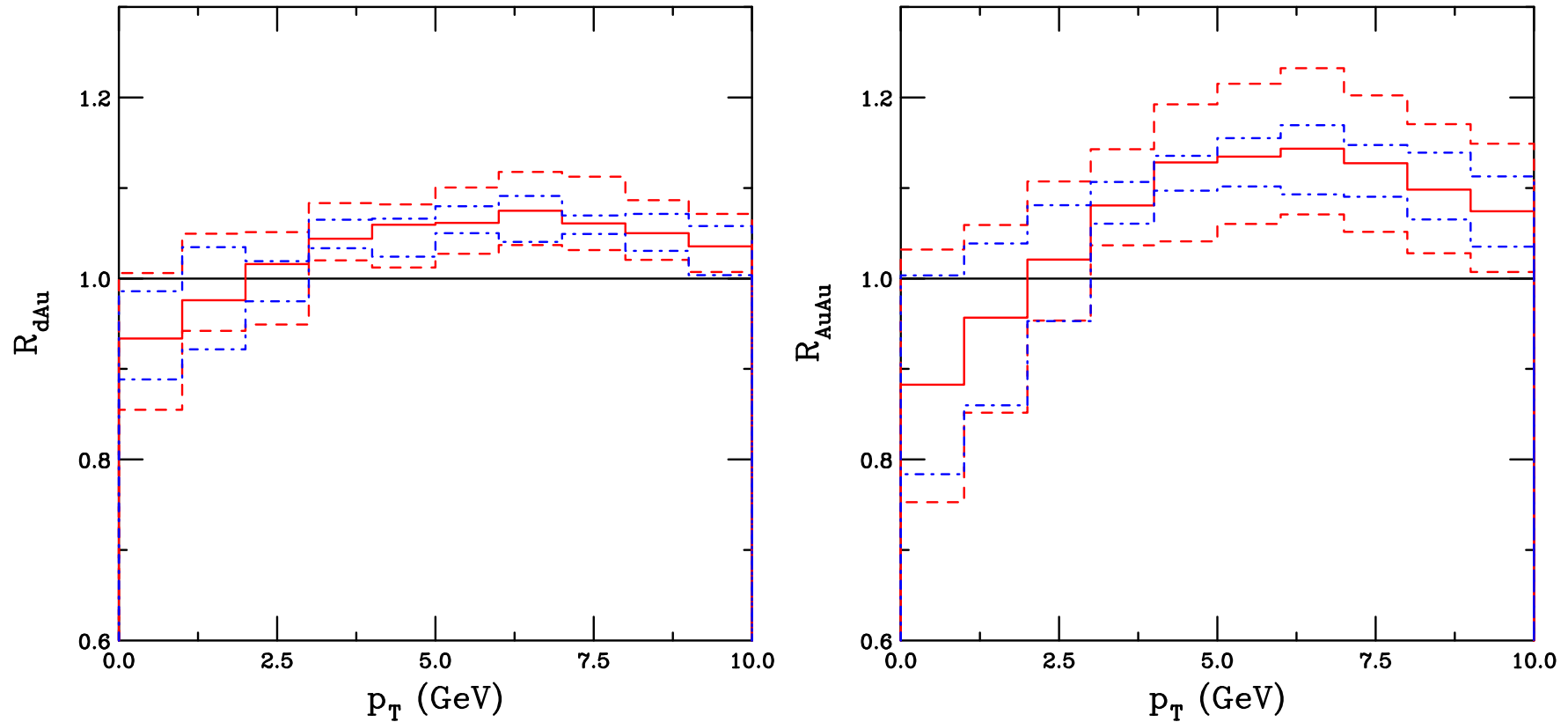


Figure 14: The ratio  $R_{dAu}$  (left) and  $R_{AuAu}$  (right) at  $\sqrt{s} = 200$  GeV. The dashed red histogram shows the EPS09 uncertainties while the dot-dashed blue histogram shows the dependence on mass and scale.

## Summary .

- Fitting the scale parameters to the total charm cross section data significantly reduces the uncertainties on both open charm and  $J/\psi$
- Production mechanism affects interpretation of  $pA$ ,  $dA$  data
- Significant differences in cold nuclear matter effects on  $J/\psi$  between LO and NLO shadowing with EPS09 parameterization

# Backup

# Why CEM?

Open and hidden charm photo- and hadroproduction show similar energy dependence

High  $p_T$  Tevatron Run I data show that, within uncertainties of the data, the prompt  $J/\psi$ , the  $\psi'$  and  $\chi_c$   $p_T$  dependencies are the same

Amundsen *et al.* calculated partial  $p_T$  distribution (only real part) harder than data at high  $p_T$ , undershoots at low  $p_T$  – likely because they do not include any  $k_T$  smearing

Gavai *et al.* calculated complete  $J/\psi$   $p_T$  distribution starting from exclusive NLO  $Q\bar{Q}$  production code by Mangano *et al.*

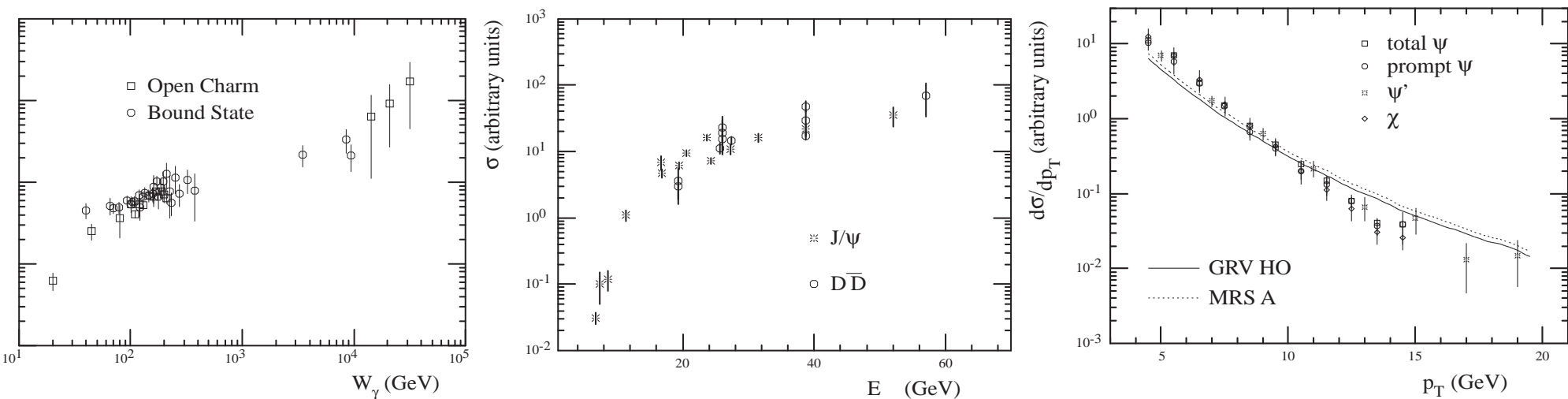


Figure 15: (Left) Photoproduction data as a function of the photon energy in the hadron rest frame,  $W_\gamma$ . (Center) Hadroproduction data as a function of the center-of-mass energy,  $E_{\text{cm}}$ . In both cases, the normalization has been adjusted to show the similar shapes of the data. (Right) Run I data from the CDF Collaboration, shown with arbitrary normalization. The curves are the predictions of the color evaporation model at tree level, also shown with arbitrary normalization. [Amundson *et al.*]

# Uncertainty Due to Gluon Densities

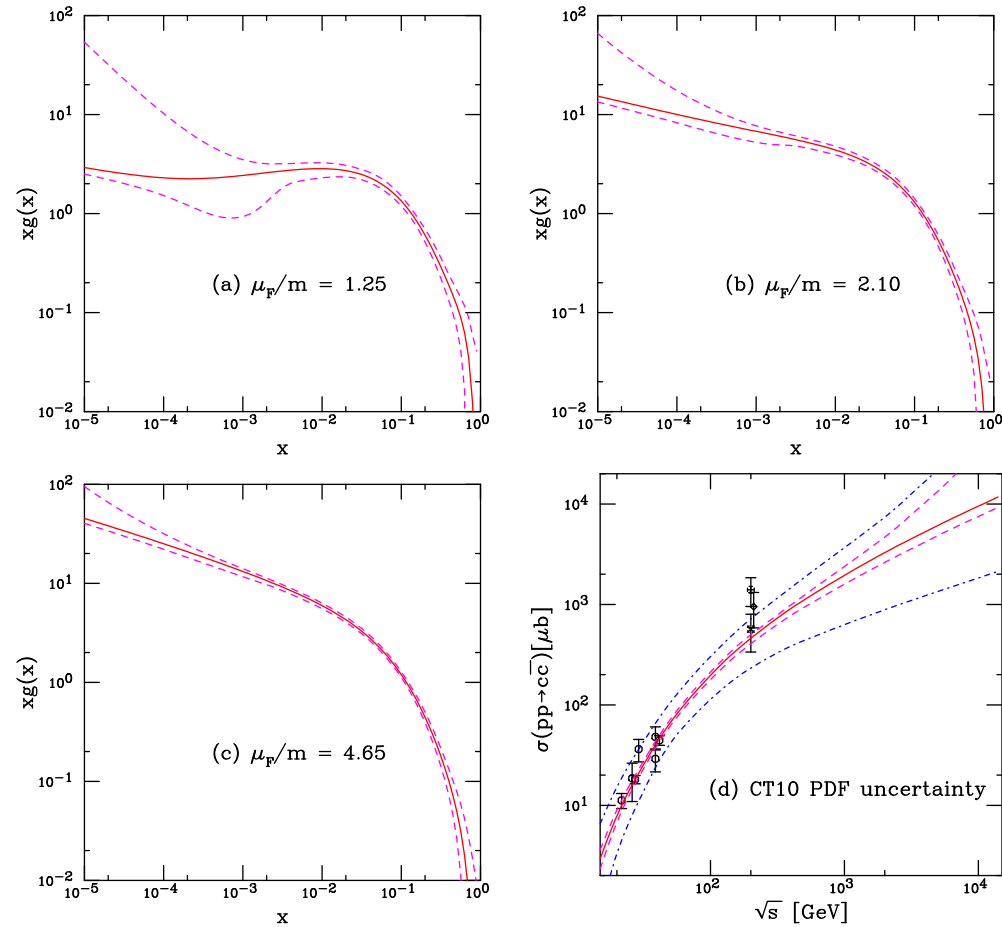


Figure 16: The CT10 gluon distribution,  $xg(x, \mu_F)$ , is shown for the relevant values of  $\mu_F/m$  for the total cross section calculation. The central value of the CT10 gluon distribution is given in the red solid curve while the uncertainty band is denoted by the dashed magenta curves. The results are shown for the lower limit of  $\mu_F/m$ ,  $\mu_F/m = 1.25$  (top left); the central value,  $\mu_F/m = 2.1$  (top right); and the upper limit,  $\mu_F/m = 4.65$  (bottom left). (bottom right) The corresponding uncertainty on the total charm cross section due to the uncertainty in the CT10 gluon distribution is denoted by the dashed magenta lines. The total uncertainty due to the mass and scale uncertainty as well as the gluon uncertainty combined in quadrature is given by the dot-dashed blue curves.

# Results for Heavy Flavor Distributions I: RHIC

Despite narrower uncertainty band for charm (left), relatively good agreement with PHENIX data is obtained (right)

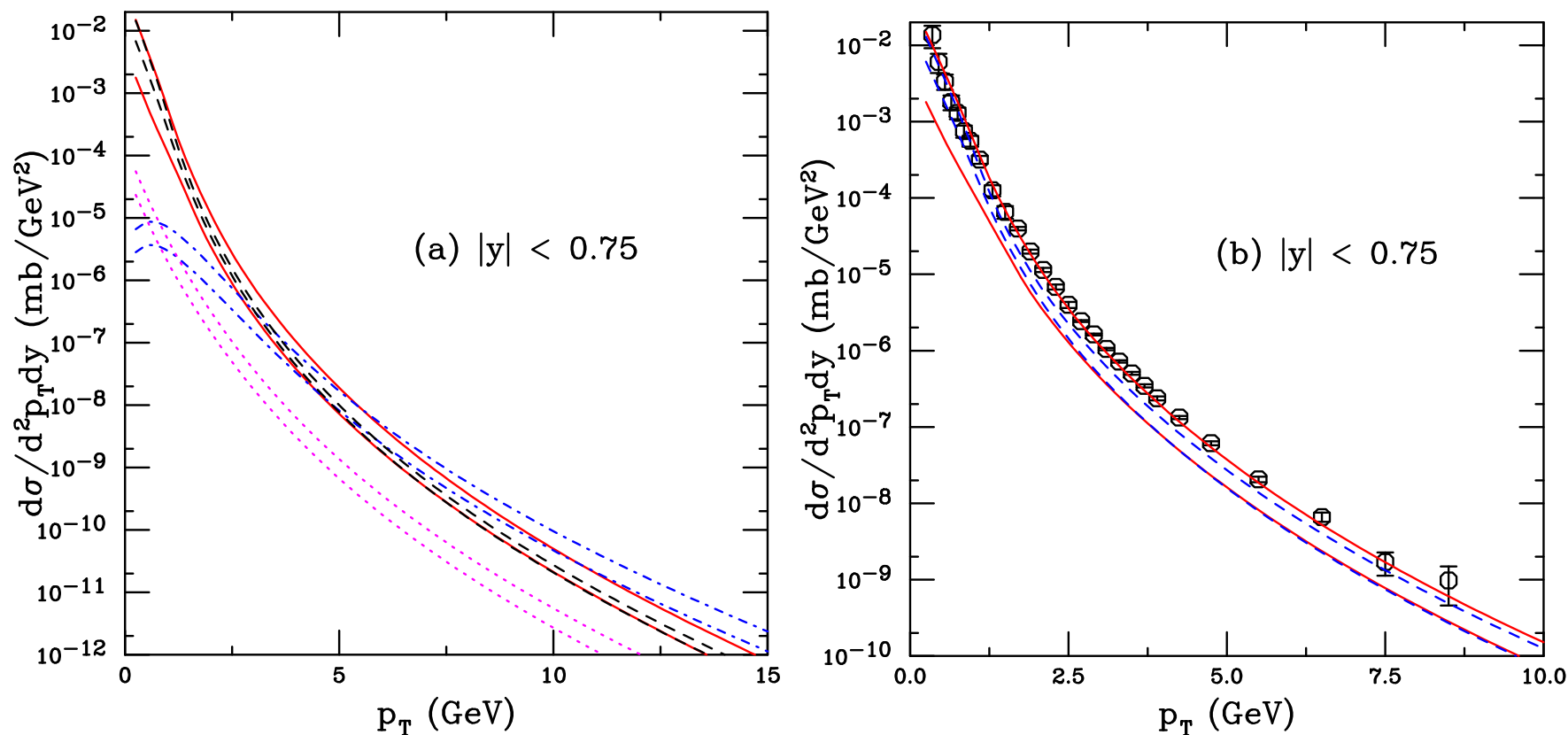


Figure 17: (Color online) (a) The components of the non-photonic electron spectrum:  $B \rightarrow e$  (dot-dashed blue);  $B \rightarrow D \rightarrow e$  (dotted magenta);  $D \rightarrow e$  both with the FONLL parameters (solid red) and those for  $m = 1.27$  GeV (dashed black) at  $|y| < 0.75$  in  $\sqrt{s} = 200$  GeV  $pp$  collisions. (b) The sum of the contributions are compared with the FONLL set for charm (solid red) and  $m = 1.27$  GeV (dashed blue). The PHENIX data are also shown.

# CEM $p_T$ Distributions

Without intrinsic  $k_T$  smearing (or resummation) the  $Q\bar{Q}$   $p_T$  distribution (LO at  $\mathcal{O}(\alpha_s^3)$  while total cross section is NLO at this order) is too peaked at  $p_T \rightarrow 0$ , needs broadening at low  $p_T$

Implemented by Gaussian  $k_T$  smearing,  $\langle k_T^2 \rangle_p = 1 \text{ GeV}^2$  for fixed target  $pp$  and  $\pi p$ , broadened for  $pA$  and  $AA$ , NLO code adds in final state:

$$g_p(k_T) = \frac{1}{\pi \langle k_T^2 \rangle_p} \exp(-k_T^2 / \langle k_T^2 \rangle_p)$$

Broadening should increase with energy we make a simple linear extrapolation to obtain

$$\langle k_T^2 \rangle_p = 1 + \frac{1}{3n} \ln \left( \frac{\sqrt{s}}{\sqrt{s_0}} \right) \text{ GeV}^2$$

We find  $n \sim 4$  agrees best with RHIC data

Note that unlike FONLL-like calculation of single inclusive heavy flavor with resummed logs of  $p_T/m$ , at large  $p_T$  distribution may be harder than it should be